

Exploring Lifshitz transition and superconductivity in 3R-NbS_2 under pressure

Kun Chen(陈坤), Xindeng Lv(吕心邓), Simin Li(李思敏), Yanping Huang(黄艳萍), and Tian Cui(崔田)

Citation: Chin. Phys. B, 2025, 34 (**3**): 037403. DOI: 10.1088/1674-1056/adacd2
Journal homepage: http://cpb.iphy.ac.cn; http://iopscience.iop.org/cpb

What follows is a list of articles you may be interested in

Coevolution of superconductivity and Hall coefficient with anisotropic lattice shrinkage in compressed $KCa_2Fe_4As_4F_2$

Jinyu Han(韩金宇), Wenshan Hong(洪文山), Shu Cai(蔡树), Jinyu Zhao(赵金瑜), Jing Guo(郭静), Yazhou Zhou(周亚洲), Pengyu Wang(王鹏玉), Lixin Cao(曹立新), Huiqian Luo(罗会仟), Shiliang Li(李世亮), Qi Wu(吴奇), and Liling Sun(孙力玲)
Chin. Phys. B, 2024, 33 (**7**): 077402. DOI: 10.1088/1674-1056/ad4d65

Robust T_c in element molybdenum up to 160 GPa

Xinyue Wu(吴新月), Shumin Guo(郭淑敏), Jianning Guo(郭鉴宁), Su Chen(陈诉), Yulong Wang(王煜龙), Kexin Zhang(张可欣), Chengcheng Zhu(朱程程), Chenchen Liu(刘晨晨), Xiaoli Huang(黄晓丽), Defang Duan(段德芳), and Tian Cui(崔田)
Chin. Phys. B, 2024, 33 (**4**): 047406. DOI: 10.1088/1674-1056/ad2a78

First-principles study of moderate phonon-mediated pairing in high-pressure monoclinic phase of BiS_2-based superconductors

Jie Cheng(程杰), Yu-Lan Cheng(程玉兰), Bin Li(李斌), and Sheng-Li Liu(刘胜利)
Chin. Phys. B, 2023, 32 (**10**): 107401. DOI: 10.1088/1674-1056/accd56

A ten-fold coordinated high-pressure structure in hafnium dihydrogen with increasing superconducting transition temperature induced by enhancive pressure

Yan-Qi Wang(王妍琪), Chuan-Zhao Zhang(张传钊), Jin-Quan Zhang(张金权), Song Li(李松), Meng Ju(巨濛), Wei-Guo Sun(孙伟国), Xi-Long Dou(豆喜龙), and Yuan-Yuan Jin(金园园)
Chin. Phys. B, 2023, 32 (**9**): 097402. DOI: 10.1088/1674-1056/acc934

Focused-ion-beam assisted technique for achieving high pressure by uniaxial-pressure devices

Di Liu(刘迪), Xingyu Wang(王兴玉), Zezhong Li(李泽众), Xiaoyan Ma(马肖燕), and Shiliang Li(李世亮)
Chin. Phys. B, 2023, 32 (**4**): 047401. DOI: 10.1088/1674-1056/acac1a

---

SPECIAL TOPIC — Structures and properties of materials under high pressure

Exploring Lifshitz transition and superconductivity in 3R-NbS_2 under pressure

Kun Chen(陈坤)[1], Xindeng Lv(吕心邓)[1], Simin Li(李思敏)[1], Yanping Huang(黄艳萍)[1,†], and Tian Cui(崔田)[1,2]

[1] *Institute of High Pressure Physics, School of Physical Science and Technology, Ningbo University, Ningbo* 315211, *China*
[2] *State Key Laboratory of Superhard Materials, College of Physics, Jilin University, Changchun* 130012, *China*

(Received 29 December 2024; revised manuscript received 20 January 2025; accepted manuscript online 22 January 2025)

The interplay between electronic topological phase transitions and superconductivity in the field of condensed matter physics has consistently captivated researchers. Here we have succeeded in modulating the Lifshitz transition by pressure and realized superconductivity. At 25.7 GPa, superconductivity with a transition temperature of 1.9 K has been observed in 3R-NbS_2. The Hall coefficient changes from negative to positive at 14 GPa, indicating a Lifshitz transition in 3R-NbS_2, and the carrier concentration continues to increase with increasing pressure. X-ray diffraction results indicate that the appearance of superconductivity cannot be attributable to structural transitions. Based on theoretical calculations, the emergence of a new band is attributed to the Lifshitz transition and the new band coincides with the Fermi surface at the pressure of 30 GPa. These findings provide new insights into the relationship between the Lifshitz transition and superconductivity.

Keywords: high pressure, superconductivity, Lifshitz transition, 3R-NbS_2

PACS: 74.70.–b, 07.35.+k, 91.60.Gf, 71.18.+y

DOI: 10.1088/1674-1056/adacd2 **CSTR:** 32038.14.CPB.adacd2

1. Introduction

In condensed matter physics, a topological phase transition is characterized by changes in topological invariants, such as the Chern number and the Z_2 topological number.[1,2] Unlike conventional symmetry-breaking phase transitions, topological phase transitions do not rely on local symmetry breaking; instead, they arise from alterations in the topological nature of the electronic band structure.[3–5] Moreover, Lifshitz transitions represent a specific class of topological electronic phase transitions that are intrinsically linked to the topological characteristics of the electronic energy band structure.[6,7] These transitions involve topological changes on the Fermi surface of a material when external conditions, such as pressure,[8,9] doping,[10] magnetic field,[11] or temperature,[6,12] change, leading to phenomena such as metal–insulator transitions,[13] ferromagnetic–antiferromagnetic transitions,[14] and abrupt changes in thermodynamic quantities like heat capacity,[15] as well as exotic behaviors. During a Lifshitz transition, a new band may intersect the Fermi surface, leading to a topological reconfiguration of the Fermi level by introducing additional pockets associated with the new band. This topological reorganization can lead to significant changes in the density of states (DOS) at the Fermi level, which in turn affects the electron–electron interactions and thus the conductivity of the material, especially in strongly correlated electronic systems.[16] In these systems, the emergence of a new band may enhance the effective mass of the electrons, thereby influencing the conductivity and other electronic properties, including those of high-temperature superconductors.[17,18] Consequently, the relationship between Lifshitz transitions offers valuable insights into the changes in electronic structures of materials.

The recent discovery of ultra-flat band, which gives rise to strongly correlated states and superconductivity in twisted bilayer graphene, has sparked significant interest in investigating superconductivity through changes of electronic energy bands in layered materials.[19] Therein, transition metal dichalcogenides (TMDs), a class of layered materials, have garnered significant research attention over the past two decades. The unique structural characteristics of TMDs give rise to a diverse array of physical phenomena, including superconductivity, Mott insulating states, magnetoresistance, and charge density waves (CDW).[20–25] TMDs crystallize in two primary structural polymorphs: the hexagonal (2H) and trigonal (1T) phases. These layered structures consist of metal atoms coordinated by either trigonal prismatic (2H) or octahedral (1T) arrangements of chalcogen atoms.[26] Among TMDs, NbS_2 exhibits unique characteristics. Unlike other group V TMDs such as TaS_2,[27] $NbSe_2$,[9,28] and $TaSe_2$,[29] the 2H polymorph of NbS_2 does not undergo structural instability at low temperatures, consequently without the formation of charge density waves owing to the large anharmonic effects.[29,30] Furthermore, 2H-NbS_2 exhibits a superconducting transition temperature (T_c) of approximately 6 K at ambient pressure.[31]

†Corresponding author. E-mail: huangyanping@nbu.edu.cn

© 2025 Chinese Physical Society and IOP Publishing Ltd. All rights, including for text and data mining, AI training, and similar technologies, are reserved.

Scanning tunneling microscopy (STM) measurements reveal that 2H-NbS_2 possesses two superconducting energy gaps, indicating that it is a multiband superconductor.[31] However, superconductivity was not observed in other phases of NbS_2, such as 1T and 3R structures.[32]

It is well established that pressure can alter the properties of materials by modifying their crystal structure and electronic configuration.[33–36] For 2H-NbS_2, pressure increases the T_c from 6 K at ambient pressure to 8.9 K at 20 GPa. However, the upper critical magnetic field does not vary monotonically with pressure, likely due to pressure-induced changes in the Fermi surface.[37] Current research primarily focuses on the 2H phase, with limited studies conducted on the 3R phase.[38] Moreover, angle-resolved photoemission spectroscopy indicates greater energy band filling in 3R-NbS_2.[38] This increased band filling enhances the interaction between electrons and facilitates the exploration of various electronic phenomena. Therefore, 3R-NbS_2 provides an excellent platform to study the interaction between electrons.

In this work, we have comprehensively investigated the structural and electronic properties of 3R-NbS_2 under high pressure by synchrotron x-ray diffraction (XRD), electron transport measurements and Hall experiments. Electron transport measurements reveal the superconductivity of 3R-NbS_2 at about 25.7 GPa. Hall experiments show a Lifshitz transition in 3R-NbS_2 at 14 GPa and a continuous increase in carrier concentration with increasing pressure. XRD results indicate that the superconducting transition is not accompanied by any structural phase transition. Comprehensive calculations indicate that the appearance of superconductivity can be attributed to the pressure-induced increase of DOS near the Fermi surface.

2. Method

2.1. High-pressure experiments

The 3R-NbS_2 powder was purchased from Nanjing MKNANO Tech. Co., Ltd. Sample purity of 99.99% was achieved and was directly used after purchase without further purification. High-pressure electrical transport and Hall measurements were conducted using a symmetric Be–Cu alloy diamond anvil cell (DAC) and diamond with an anvil size of 200 μm. Resistance and Hall measurements were performed using the quasi-quadruple-probe method. We used tungsten for the gasket and pre-compressed it to about 25 GPa, then punched a 120 μm hole right at the center of the gasket. A mixture of aluminum oxide and epoxy resin was filled into the hole and re-pressurized to 30 GPa to ensure that it is firmly in the hole and to insulate the platinum electrodes from the gasket. Then an 80 μm hole was drilled for the sample chamber. The sample was placed as close as possible to the center of the sample chamber to prevent uncertainty due to potential pressure gradients. A small pressure (not exceeding 1 GPa) was applied to ensure intact contact between the sample and the platinum probes. A ruby with a diameter of no more than 10 μm was selected and positioned in the space between the electrodes in the sample chamber. For all measurements, we determined the pressure by the ruby fluorescence method and the edge of diamond Raman signal.[39,40]

In situ high-pressure x-ray diffraction (XRD) experiments on 3R-NbS_2 powder samples were conducted at the Shanghai Synchrotron Radiation Facility (SSRF) BL15U1 beamline (20 keV, 0.6199 Å). We also used a pair of diamonds with anvil sizes of 200 μm to generate the high pressure. A tungsten foil gasket was used, the tungsten sheet was pre-indented to a thickness of 45 μm, a 100 μm hole was drilled at the center of the indentation using a laser punch for the sample chamber, and a ruby with a diameter of less than 10 μm was employed as the pressure calibrator. The XRD images were integrated and analyzed using the Dioptas software package.[41] The diffraction patterns were refined by the GSAS-II.[42]

2.2. Theoretical calculations

Structural optimization and electronic properties calculations were carried out using density functional theory (DFT) with the Perdew–Burke–Ernzerhof (PBE) of generalized gradient approximation (GGA), as implemented in the Vienna *Ab initio* Simulation Package (VASP) code. The ion–electron were described using the all-electron projector augmented wave (PAW) method with $5s^1 4d^4$ and $3s^2 3p^4$ as valence electrons for Nb and S, respectively.[43] To obtain a better energy convergence, we have chosen a plane-wave cutoff energy of 650 eV and Monkhorst–Pack k-meshes of $2\pi \times 0.02^{-1}$ to ensure the enthalpy converging to less than 1 meV/atom.

3. Results and discussion

At ambient pressure, the 3R phase exhibits the $R3m$ space group (No. 160); it consists of a multilayered S–Nb–S sandwich structure stacked with layers connected by van der Waals forces and predominantly covalent bonds within the layers; and the relative translation between layers is one third of the lattice constant.[38] In contrast to the 2H phase, there is not a center of inversion symmetry between the layers (Fig. 1(a)). To verify the purity and crystal structure of the purchased 3R-NbS_2, we first conducted x-ray diffraction (XRD) measurement using Mo $K\alpha$ radiation ($\lambda = 0.7107$ Å) with a Rigaku Nanopix WE instrument under ambient conditions, and the results are shown in Fig. 1(b). It can be observed that the Bragg peaks in the diffraction pattern correspond well with the NbS_2 structure adopting $R3m$ space group. Additionally, to investigate whether the sample exhibits superconductivity under ambient pressure, we performed electrical resistance measurements. As shown in Fig. 1(c), the samples exhibit good metallic properties. Notably, no signs of superconductivity are observed in the sample within the temperature range of 1.7 K to

300 K, which is consistent with previous studies.[38]

To explore the electrical properties of 3R-NbS_2 under high pressure, we conducted high-pressure electrical resistance measurements, and the results are illustrated in Fig. 2. At 0.8 GPa, 3R-NbS_2 displays a typical metallic behavior. With the pressure increasing, we observed a gradual decrease in resistance over the entire temperature range, a trend that persists up to 22.6 GPa (Fig. 2(a)). Upon further compression to 25.7 GPa, a sudden drop in resistance occurs at approximately 1.9 K, indicating a potential superconducting transition in 3R-NbS_2. At the same time, the appearance of superconductivity is accompanied by an increase in normal state resistance (Figs. 2(b) and 2(c)), which was also observed in the other TMDs.[44,45] As pressure increases, the drop in resistance becomes more pronounced, and the sample reaches a zero-resistance state at 63.5 GPa (Fig. 2(d)). The pressure dependence of T_c can be divided into two distinct regions. Below 53 GPa, T_c remains nearly constant, showing minimal variation with increasing pressure. However, T_c experiences a notable upsurge, escalating from 2.5 K to 5.6 K within the pressure interval from 53 GPa to 76 GPa, without manifesting any signs of saturation (inset in Fig. 2(c)). Therefore, subsequent studies imposing higher pressures are expected to obtain high transition temperatures for superconductivity.[46] Corresponding observations have been observed in 2H-NbS_2, attributed to changes in the Fermi surface. Furthermore, to verify that the resistance drop of 3R-NbS_2 was due to the superconducting transition, we performed transport measurements under varying external magnetic fields at 63.5 GPa. As shown in Fig. 2(e), as the magnetic field increases in the 0–2 T range, T_c is obviously suppressed to a lower temperature, further confirming the superconductivity of the sample. The upper critical field is extrapolated using the single-band Werthamer–Helfand–Hohenberg (WHH) formula and the Ginzburg–Landau (GL) equation,[47] where the estimated values of $\mu_0 H_{c2}(0)$ are 3.37 T and 3.96 T, respectively. These values do not exceed the Pauli paramagnetic limit of $\mu_0 H_p(0) = 1.84 T_c \approx 7$ T for $T_c = 3.8$ K.[48]

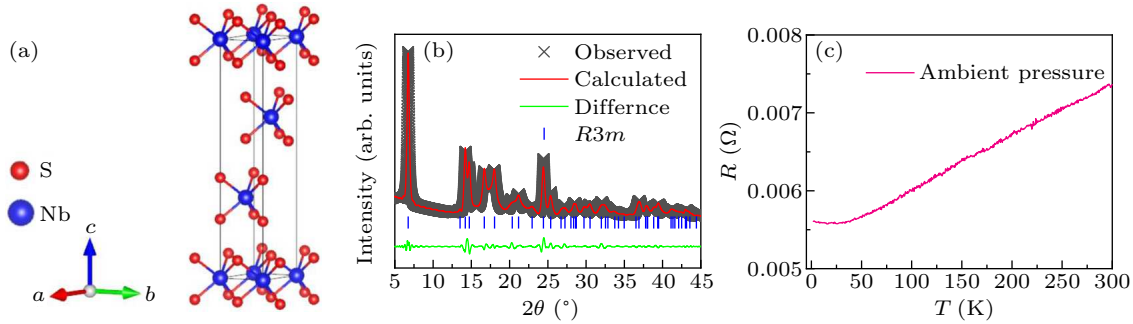


Fig. 1. Structure and electronic transport properties of 3R-NbS_2 at ambient pressure. (a) Crystal structure of 3R-NbS_2. The red and blue balls represent the S and Nb atoms, respectively. (b) Rietveld refinement of 3R-NbS_2. (c) Temperature dependence of resistance for 3R-NbS_2.

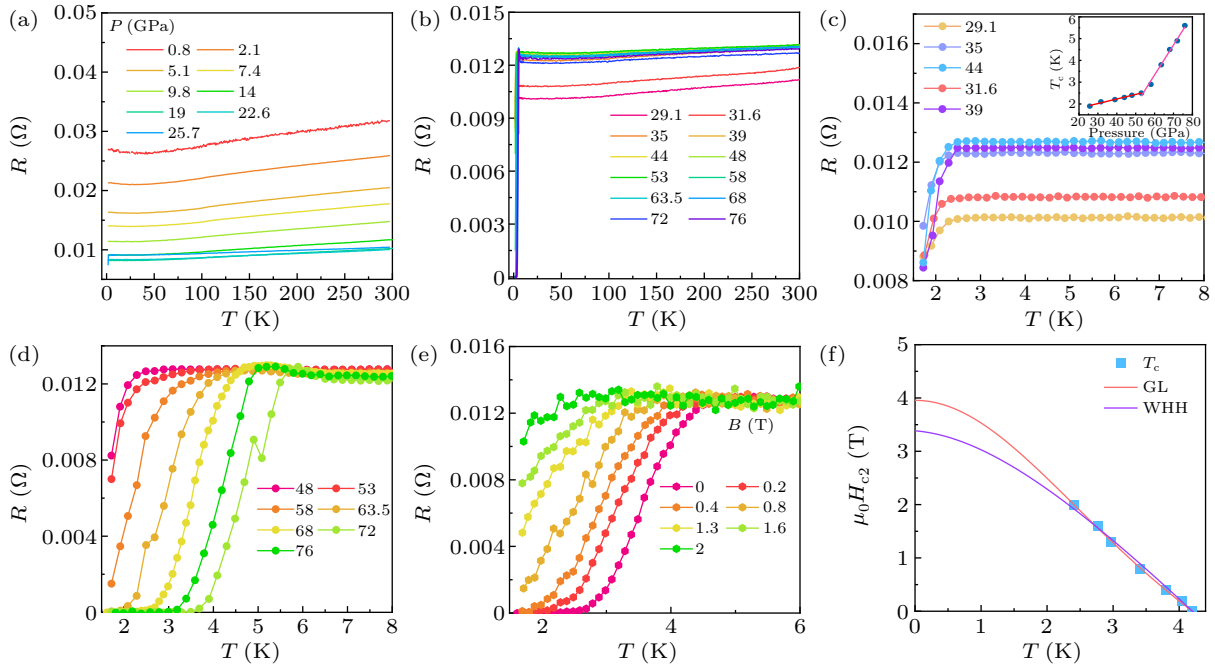


Fig. 2. (a) Electrical resistance of 3R-NbS_2 as a function of temperature below 25.7 GPa and (b) above 29.1 GPa. (c) and (d) Temperature-dependent resistance of 3R-NbS_2 in the vicinity of superconductivity with different pressure ranges. (e) Temperature dependence of resistance under various magnetic fields for 3R-NbS_2 at 63.5 GPa. (f) Temperature dependence of upper critical field $\mu_0 H_{c2}$ at 63.5 GPa. The solid lines represent the Ginzburg–Landau (GL) and Werthamer–Helfand–Hohenberg (WHH) fittings.

To further comprehend the superconductivity of 3R-NbS_2 under pressure, we performed high pressure Hall measurements by applying an external magnetic field from −3 T to +3 T to the sample. Figure S1 shows the Hall resistance R_{xy} as a function of H at different pressures at 10 K. We extracted the Hall coefficients (R_H) from the Hall resistance $R_{xy}(H)$ and established the function of R_H with pressure. As shown in Fig. 3(a), R_H is overall negative below 14 GPa, reflecting that the electron carriers are dominant. In addition, the R_H changes from negative to positive at 14 GPa, indicating a shift in the dominant carrier type from electrons (n-type) to holes (p-type). The changed sign of the R_H with pressure suggests that the Fermi surface of 3R-NbS_2 undergoes a possible reconstruction that can be seen as a sign of a Lifshitz transition.[49,50] To investigate the variation of carrier concentration with pressure, we estimated the carrier concentration using the single-band Drude model $n = -1/(eR_H)$ based on the linear relationship between R_{xy} and $\mu_0 H$. As shown in Fig. 3(b), the carrier concentration shows a sudden increase at 14 GPa, followed by a rapid rise with increasing pressure. The increase in carrier concentration implies that more electrons are involved in the inter-electron interactions. It is possible that the enhanced inter-electron interactions are the dominant factor in the evolution of 3R-NbS_2 conductivity.

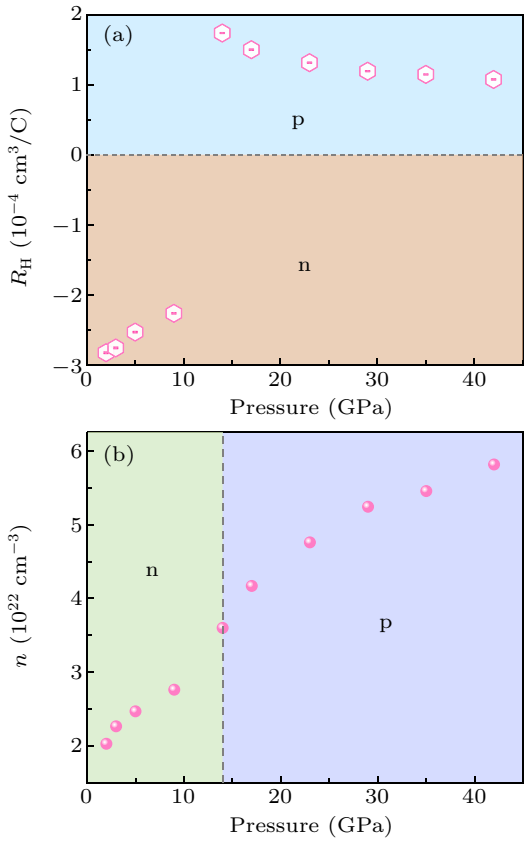


Fig. 3. Hall effect of 3R-NbS_2 under high pressures. (a) Pressure-dependent Hall coefficient R_H of 3R-NbS_2. High-pressure Hall measurements were carried out using the van der Pauw method. (b) Pressure-dependent carrier concentration (n) of 3R-NbS_2.

To check whether the superconductivity of 3R-NbS_2 originates from a structural phase transition, we carried out high-pressure *in situ* XRD measurements at various pressures under room temperature. Figure 4(a) presents the XRD patterns of 3R-NbS_2 under high pressures, ranging from 0.8 GPa to 59.8 GPa. We found that as the crystal is compressed, the peak shifts towards higher angles without the emergence of new peaks (Fig. S2), indicating that 3R-NbS_2 does not undergo pressure-induced structural phase transitions up to 59.8 GPa. To assess the mechanical behavior under compression, we analyzed the unit cell volume and lattice parameters as functions of pressure. As shown in Figs. 4(b) and 4(c), the sample exhibits significant anisotropy, with the c-axis demonstrating a substantially higher compression rate compared to the a-axis. Concurrently, both the lattice parameters and the unit cell volume decrease progressively with increasing pressure, without any indication of discontinuity across the measured pressure range. Fitting the P–V data using the third-order Birch–Murnaghan (BM) equation of state[51] yields a volume at ambient pressure of $V_0 = 174(1)$ Å^3, a bulk modulus at ambient pressure of $B_0 = 80.2(2)$ GPa, and the first-order derivative of the bulk modulus at ambient pressure of $B_0' = 10.7(2)$ close to previous studies.[52] Therefore, the *in situ* high-pressure XRD results indicate that the pressure induced superconductivity in 3R-NbS_2 is not associated with a structural phase transition (Fig. 4(d)).

Pressure can modify not only the structure but also the electronic structure of the material. Therefore, to better understand the reasons behind the emergence of superconductivity in 3R-NbS_2, we conducted first-principles computational analyses to calculate its electronic band structure and density of states, as shown in Fig. 5. Figure 5(a) illustrates the band structure of 3R-NbS_2 at ambient pressure, which exhibits the typical metallic behavior and reveals three interconnected bands traversing the Fermi level, resulting in the formation of electron-type and hole-type Fermi pockets. At 15 GPa, an energy band from near the G point below the Fermi surface at 0 GPa is observed to cross the Fermi level along the K–Γ–M direction, forming a new hole Fermi pocket (Fig. 5(b)), suggesting that the material undergoes an electronic phase transition, specifically a Lifshitz transition. Interestingly, at 30 GPa (Fig. 5(c)), we observed the energy band near the Γ point, located close to the Fermi level, which resembles flat band leading to a substantial increase in the DOS.[53] This high DOS provides favorable conditions for strong electron–electron interactions, potentially facilitating electron pairing and the emergence of superconductivity. As shown in Fig. 5(d), a sharp peak in the DOS near the Fermi level creates the necessary conditions for superconductivity to develop. To better illustrate the evolution of the electronic structure under pressure, we plotted the PDOS of the S atom at 0 GPa, 15 GPa, and 30 GPa in Fig. 5(h). It can be seen that the contribution of the S_p orbital to the Fermi level gradually increases with increasing pressure. In addition, the 3D

Fermi surface at different pressures is shown in Figs. 5(e)–5(g). At 15 GPa, a new flattened Fermi pocket appears at the center of the Brillouin, suggesting that a Lifshitz transition occurs, and the new Fermi pocket grows larger with the increase of the pressure, which is in agreement with the results of our Hall measurements. Thus, the emergence of 3R-NbS_2 superconductivity is closely related to topological changes on the Fermi level.

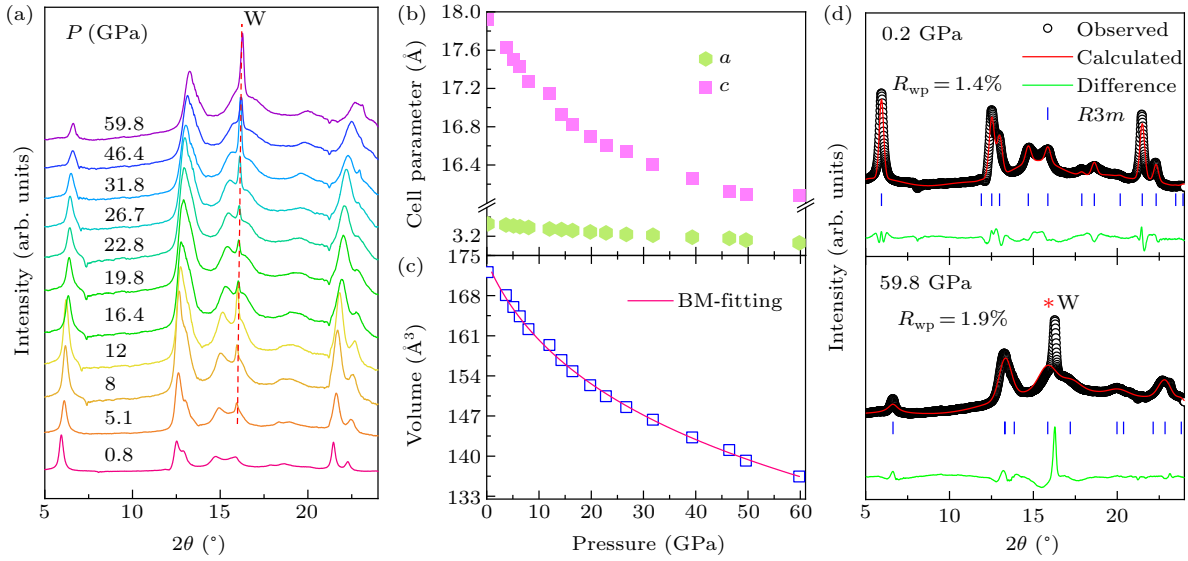


Fig. 4. XRD results of 3R-NbS_2 under high pressure at room temperature. (a) XRD patterns of 3R-NbS_2 collected at different pressures. The dashed line indicates the variation of the tungsten peak with pressure. (b) Cell parameters as a function of pressure. (c) Pressure-dependent unit cell volume. (d) Rietveld refinements for 3R-NbS_2 at 0.2 GPa and 59.8 GPa, respectively ($\lambda = 0.6199$ Å). The asterisks in the lower panel represent tungsten peaks.

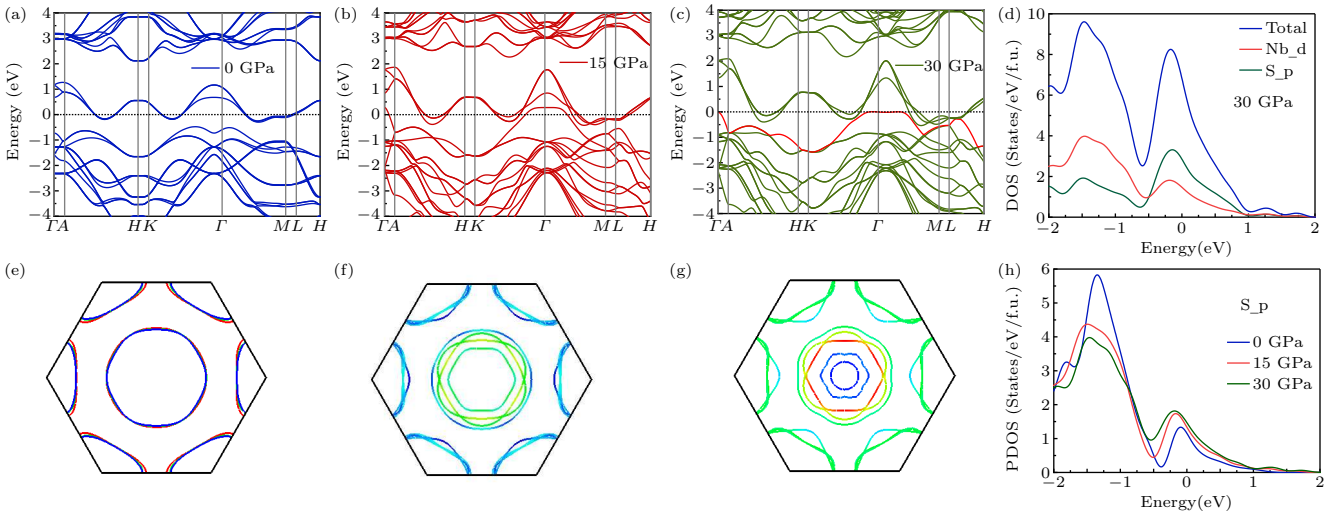


Fig. 5. The calculated electronic band structure at (a) 0 GPa, (b) 15 GPa, (c) 30 GPa. (d) The calculated DOS at 30 GPa. (e)–(g) 3D Fermi surface of 3R-NbS_2 at 0 GPa, 15 GPa, and 30 GPa, respectively. (h) The PDOS of the S atomic p-orbitals at 0 GPa, 15 GPa, and 30 GPa.

Phase diagrams were constructed based on high-pressure electrical transport and XRD measurements, as illustrated in Fig. 6. No structural transition was observed up to 60 GPa. At the temperature of 297 K, the resistance initially decreases with increasing pressure but begins to increase as the pressure approaches the critical point for the emergence of superconductivity. This resistance behavior is predominantly governed by electron–phonon scattering. Notably, the pressure-dependent variation of the T_c exhibits two distinct stages. Initially, the increase is gradual, but it becomes more pronounced at pressures exceeding 53 GPa. The underlying reasons for this phenomenon require further investigation.

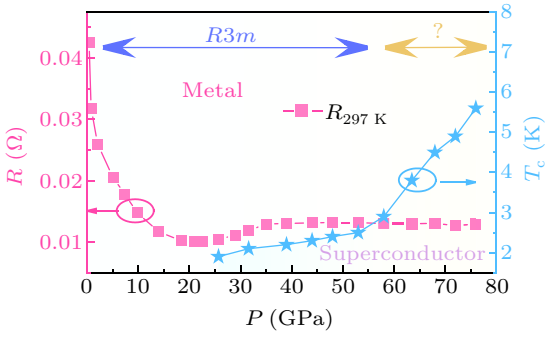


Fig. 6. Pressure–temperature (P–T) phase diagram of 3R-NbS_2.

4. Conclusion

We have reported the pressure-induced superconductivity in 3R-NbS_2. The T_c increases with the application of pressure; however, the rate of change of T_c with pressure differs significantly below and above 53 GPa, with maximum $T_c \sim 5.6$ K at 76 GPa. The Hall measurements indicate that the Hall coefficient changes from negative to positive at 14 GPa, which is a sign of the Lifshitz transition, and the carrier concentration continues to increase sustainably with increasing pressure after the abrupt increase at 14 GPa. *In-situ* XRD measurements results show no crystal structural transition at the emergence of superconductivity. Combination of experimental data and calculations indicates that the onset of superconductivity in 3R-NbS_2 under pressure can be attributed to the effective modulation of its electronic structure. The Lifshitz transition induces a new band closer to the Fermi level with increasing pressure. This further enhances the DOS and promotes the formation of electron pairs playing a key role in the superconductivity. We report the first high-pressure experimental study of 3R-phase pressure-induced superconductivity without structural transition in TMDs, providing new insights and sufficient experimental evidence that pressure-induced superconductivity can be achieved without altering the crystal structure, but by modulating the electronic structure.

Acknowledgments

Project supported by the National Key R&D Program of China (Grant No. 2022YFA1405500), the National Natural Science Foundation of China (Grant Nos. 52072188 and 12304072), Program for Science and Technology Innovation Team in Zhejiang (Grant No. 2021R01004), and the Natural Science Foundation of Ningbo (Grant No. 2021J121).

References

[1] Kane C L and Mele E J 2005 *Phys. Rev. Lett.* **95** 146802
[2] Yin J, Ma W, Cochran T A, *et al.* 2020 *Nature* **583** 533
[3] Xu S, Xia Y, Wray L A, Jia S, Meier F, Dil J H, Osterwalder J, Slomski B, Bansil A, Lin H, Cava R J and Hasan M Z 2011 *Science* **332** 560
[4] Xu S, Liu C, Alidoust N, *et al.* 2012 *Nat. Commun.* **3** 1192
[5] Verbin M, Zilberberg O, Kraus Y E, Lahini Y and Silberberg Y 2013 *Phys. Rev. Lett.* **110** 076403
[6] Wu Y, Jo N H, Ochi M, Huang L, Mou D, Bud'ko S L, Canfield P C, Trivedi N, Arita R and Kaminski A 2015 *Phys. Rev. Lett.* **115** 166602
[7] Zhang Y, Wang C, Yu L, *et al.* 2017 *Nat. Commun.* **8** 15512
[8] Chi Z, Zhang J, Gong Z, Peng F, Wang X, Dong G, Li Y, Shi Y, Ge Y, Yang X, Zhang Z, Xu G, Hao N, Zhou C and Qin J 2024 *Mater. Today Phys.* **42** 101372
[9] Nishimura T, Sakai H, Mori H, *et al.* 2019 *Phys. Rev. Lett.* **122** 226601
[10] Ghosh A, Ghosh H and Sen S 2019 *Intermetallics* **107** 126
[11] Schlottmann P 2011 *Phys. Rev. B* **83** 115133
[12] Li Q, Wang B, Tang N, Li C, Yi E, Shen B, Guo D, Zhong D and Wang H 2023 *Chin. Phys. Lett.* **40** 067101
[13] Dobrovits S, Kim B, Reticcioli M, Toschi A, Khmelevskyi S and Franchini C 2019 *J. Phys. Condens. Matter* **31** 244002
[14] Lee T E 2013 *Phys. Rev. Lett.* **110** 257204
[15] Zhong Y, Chen Z, Chen S, Xu K, Hashimoto M, He Y, Uchida S, Lu D, Mo S and Shen Z 2022 *Proc. Natl. Acad. Sci. USA* **119** e2204630119
[16] Beaulieu S, Dong S, Tancogne-Dejean N, Dendzik M, Pincelli T, Maklar J, Xian R P, Sentef M A, Wolf M, Rubio A, Rettig L and Ernstorfer R 2021 *Sci. Adv.* **7** enbd9275
[17] Shimizu M, Takemori N, Guterding D and Jeschke H O 2018 *Phys. Rev. Lett.* **121** 137001
[18] Tian H, Tu T, Jin X, Li C, Lin T, Dong Q, Jing X, Liu B, Liu R, Li D, Liu Z, Li Q, Peng H and Liu B 2024 *J. Am. Chem. Soc.* **146** 7324
[19] Cao Y, Fatemi V, Fang S, Watanabe K, Taniguchi T, Kaxiras E and Jarillo-Herrero P 2018 *Nature* **556** 43
[20] Wang Y, Yao W, Xin Z, Han T, Wang Z, Chen L, Cai C, Li Y and Zhang Y 2020 *Nat. Commun.* **11** 4215
[21] Ali M N, Xiong J, Flynn S, Tao J, Gibson Q D, Schoop L M, Liang T, Haldolaarachchige N, Hirschberger M, Ong N P and Cava R J 2014 *Nature* **514** 205
[22] Deng Y, Lai Y, Zhao X, Wang X, Zhu C, Huang K, Zhu C, Zhou J, Zeng Q, Duan R, Fu Q, Kang L, Liu Y, Pennycook S J, Wang X and Liu Z 2020 *J. Am. Chem. Soc.* **142** 2948
[23] Kvashnin Y, VanGennep D, Mito M, Medvedev S A, Thiyagarajan R, Karis O, Vasiliev A N, Eriksson O and Abdel-Hafiez M 2020 *Phys. Rev. Lett.* **125** 186401
[24] Sipos B, Kusmartseva A F, Akrap A, Berger H, Forró L and Tutiš E 2008 *Nat. Mater.* **7** 960
[25] Zhou M, Gu Y, Ni S, Ruan B, Liu Q, Yang Q, Chen L, Yi J, Shi Y, Chen G and Ren Z 2023 *Phys. Rev. B* **108** 224518
[26] Manzeli S, Ovchinnikov D, Pasquier D, Yazyev O V and Kis A 2017 *Nat. Rev. Mater.* **2** 17033
[27] Achari A, Bekaert J, Sreepal V, *et al.* 2022 *Nano Lett.* **22** 6268
[28] Grasset R, Cea T, Gallais Y, Cazayous M, Sacuto A, Cario L, Benfatto L and Méasson M A 2018 *Phys. Rev. B* **97** 094502
[29] Lin D, Li S, Wen J, Berger H, Forró L, Zhou H, Jia S, Taniguchi T, Watanabe K, Xi X and Bahramy M S 2020 *Nat. Commun.* **11** 2406
[30] Leroux M, Le Tacon M, Calandra M, Cario L, Méasson M A, Diener P, Borrissenko E, Bosak A and Rodière P 2012 *Phys. Rev. B* **86** 155125
[31] Guillamón I, Suderow H, Vieira S, Cario L, Diener P and Rodière P 2008 *Phys. Rev. Lett.* **101** 166407
[32] Ge W, Kawahara K, Tsuji M and Ago H 2013 *Nanoscale* **5** 5773
[33] Tian C, Gao Y, Tian F, Wang X, Zhang Z, Duan D, Huang X and Cui T 2022 *Phys. Rev. B* **105** L180506
[34] Tian C, Gao Y, Huang X, Fang Y, Huang F and Cui T 2023 *Inorg. Chem.* **62** 11626
[35] Yu F, Wen X, Gui Z, Wu T, Wang Z, Xiang Z, Ying J and Chen X 2022 *Chin. Phys. B* **31** 017405
[36] Li Q, Zhang Y, Xiang Z, Zhang Y, Zhu X and Wen H 2024 *Chin. Phys. Lett.* **41** 017401
[37] Tissen V G, Osorio M R, Brison J P, Nemes N M, García-Hernández M, Cario L, Rodière P, Vieira S and Suderow H 2013 *Phys. Rev. B* **87** 134502
[38] El Youbi Z, Jung S W, Richter C, Hricovini K, Cacho C and Watson M D 2021 *Phys. Rev. B* **103** 155105
[39] Mao H K, Xu J and Bell P M 1986 *J. Geophys. Res.* **91** 4673
[40] Akahama Y and Kawamura H 2010 *J. Phys. Conf. Ser.* **215** 012195
[41] Prescher C and Prakapenka V B 2015 *High Pressure Res.* **35** 223
[42] Toby B H and Von Dreele R B 2013 *J. Appl. Cryst.* **46** 544
[43] Blöchl P E 1994 *Phys. Rev. B* **50** 17953
[44] Dong Q, Pan J, Li S, Fang Y, Lin T, Liu S, Liu B, Li Q, Huang F and Liu B 2022 *Adv. Mater.* **34** 2103168
[45] Dong Q, Pan J, Li S, Li C, Lin T, Liu B, Liu R, Li Q, Huang F and Liu B 2023 *J. Am. Chem. Soc.* **145** 14581
[46] Zhong W, Zhang H, Karaca E, Zhou J, Kawaguchi S, Kadobayashi H, Yu X, Errandonea D, Yue B and Hong F 2024 *Phys. Rev. Lett.* **133** 066001
[47] Werthamer N R, Helfand E and Hohenberg P C 1966 *Phys. Rev.* **147** 295
[48] Clogston A M 1962 *Phys. Rev. Lett.* **9** 266
[49] Tian C, Huang X, Gao Y, Tian F, Liang M, Fang Y, Huang F and Cui T 2023 *Phys. Rev. B* **108** L180507
[50] Lv X, Song H, Chen K, Liu S, Huang Y, Fang Y, Shen Z and Cui T 2024 *Sci. Chin. Phys. Mech. Astron.* **67** 128211
[51] Birch F 1947 *Phys. Rev.* **71** 809
[52] Ehm L, Knorr K and Depmeier W 2007 *J. Alloys Compd.* **429** 82
[53] Deng S, Simon A and Köhler J 2000 *Solid State Sci.* **2** 31